Three-dimensional particle simulations of collisionless magnetic reconnection

A. Zeiler and D. Biskamp
Max-Planck-Institut für Plasmaphysik, Centre for Interdisciplinary Plasma Science, Garching, Germany

J. F. Drake, B. N. Rogers, and M. A. Shay
Institute for Plasma Research, University of Maryland, College Park, Maryland, USA

M. Scholer
Max-Planck-Institut für Extraterrestrische Physik, Centre for Interdisciplinary Plasma Science, Garching, Germany

Received 30 August 2001; revised 4 December 2001; accepted 7 December 2001; published 10 September 2002.

[1] Three-dimensional (3-D) particle simulations are performed in a double current layer configuration to investigate the stability of current sheets and boundary layers which develop during magnetic reconnection of antiparallel fields in collisionless plasma. The strong current layers that develop near the x line remain surprisingly laminar, with no evidence of turbulence and associated anomalous resistivity or viscosity. Neither the electron shear flow instabilities nor kink-like instabilities, which have been observed in these current layers in earlier simulations, are present. The sharp boundary layers which form between the inflow and outflow regions downstream of the x line are unstable to the lower hybrid drift instability. The associated fluctuations, however, do not strongly impact the rate of reconnection. As a consequence, magnetic reconnection in the 3-D system remains nearly two dimensional. *INDEX TERMS:* 7835 Space Plasma Physics: Magnetic reconnection; 7843 Space Plasma Physics: Numerical simulation studies; 2764 Magnetospheric Physics: Plasma sheet; 2724 Magnetospheric Physics: Magnetopause, cusp, and boundary layers; *KEYWORD:* magnetic reconnection instabilities

Citation: Zeiler A., D. Biskamp, J. F. Drake, B. N. Rogers, M. A. Shay, and M. Scholer, Three-dimensional particle simulations of collisionless magnetic reconnection, *J. Geophys. Res.*, *107*(A9), 1230, doi:10.1029/2001JA000287, 2002.

1. Introduction

[2] Collisionless magnetic reconnection facilitates the conversion of magnetic energy to high-velocity plasma flows, energetic beams, and thermal motion. In the case of a simple reversed magnetic field a fairly detailed understanding has been developed by comparing two-fluid, hybrid and full particle simulations [*Birn et al.*, 2001]. Nevertheless, the overall physical picture remains incomplete since this investigation was restricted to a system with spatial variation in the two-dimensional (2-D) plane perpendicular to the direction of the current. Such a model necessarily eliminates instabilities with a variation along the current sheet transverse to the plane of reconnection. A number of instabilities have been discussed as candidates for producing structure in the out-of-plane direction. These include the drift kink [*Zhu and Winglee*, 1996; *Ozaki et al.*, 1996; *Pritchett and Coroniti*, 1996; *Daughton*, 1999; *Horiuchi and Sato*, 1999] and sausage [*Büchner*, 1999] instabilities at the ion scales. These instabilities are at a large enough scale that they would substantially modulate reconnection in the out-of-plane direction. There is now substantial evidence that the prominence of the drift kink instability in early simulations was a consequence of an unrealistic electron-to-ion mass ratio and that at realistic mass ratios the drift kink mode would be suppressed [*Daughton*, 1999]. In recent 3-D particle simulations, therefore, symmetry constraints were imposed to eliminate the drift-kink instability, and the resulting simulations indicated that reconnection remained largely two-dimensional [*Hesse et al.*, 2001; *Pritchett*, 2001]. Buneman [*Krall and Trivelpiece*, 1973], lower hybrid drift [*Huba et al.*, 1980; *Brackbill et al.*, 1984; *Horiuchi and Sato*, 1999; *Pritchett and Coroniti*, 2001; *Rogers et al.*, 2000], and electron shear flow [*Drake et al.*, 1997; *Rogers et al.*, 2000] instabilities arise at smaller scales and may therefore in the nonlinear state be represented as an anomalous resistivity or viscosity. Electron shear flow instabilities specifically were found to broaden the electron current layer, which develops at the x line during collisionless reconnection to several times the electron skin depth, $d_e = c/\omega_{pe}$ [*Rogers et al.*, 2000]. Fluid simulations, however, must be interpreted with care since kinetic effects are expected to play a major role, in particular, in the vicinity of the neutral line where electrons and ions become unmagnetized. Using massively parallel computers, it becomes feasible to challenge the previous fluid results with full particle simulations and to extend earlier full particle simulations to much larger ion-to-electron mass ratios.

0148-0227/02/2001JA000287$09.00

[3] In the present paper, using a full particle simulation model, we therefore explore the growth of secondary instabilities in the current and density layers that self-consistently develop during magnetic reconnection. The goal is first to determine whether reconnection has a tendency to self-modulate in the out-of-plane direction and second to determine whether small-scale instabilities develop in these layers and produce anomalous resistivity or viscosity, which feeds back on the rate of reconnection. In this paper we will not explore the role of instabilities that develop in realistic magnetotail equilibria in triggering reconnection during substorms. For this reason we focus primarily on the late time behavior of the dynamics after the current layer near the x line and the slow shocks separating the inflow and outflow regions have approached their steady state structure. A true steady state cannot, of course, be achieved in the present simulations because computational constraints limit the macroscopic size of the system. Nevertheless, as near as we can tell, the late time results are relatively insensitive to the initial widths of the current layers. The goal is also not to obtain an asymptotic scaling of the reconnection rate. This requires the exploration of reconnection in very large systems so that the macroscopic and microscopic scales are well separated. This is not possible within the constraints of the present computer systems while at the same time achieving sufficient separation of the ion and electron inertial scale lengths and the Debye length. We do find reconnection rates that are comparable with those measured in the Geospace Environmental Modeling (GEM) Reconnection Challenge [*Birn et al.*, 2001].

[4] The high-resolution 3-D simulations have been completed on a massively parallel T3E systems with typically 250 million electrons and 250 million ions using a newly developed relativistic particle code. Our simulations confirm the importance of the lower hybrid drift instability at the boundary between the inflow and outflow regions downstream of the x line, where the gradient in the plasma pressure steepens as a result of the formation of "slow shocks." The strong current layers that develop near the x line remain surprisingly laminar. The lower hybrid drift instability, the drift kink instability and electron shear flow driven instabilities all remain stable in the vicinity of the x line. The lower hybrid drift mode is stabilized by finite β effects in the region of large density gradient, which forms very close to the x line and is also stable in the region of lower β farther from the x line, where gradients are more modest. The electron shear flow instability, however, which destabilizes narrow electron current sheets in the two-fluid limit, is totally absent in our full particle simulations. Stability is a consequence of the increased width of the electron current layers in the kinetic versus the two-fluid model. The electron heating that occurs as the electrons become demagnetized at the x line prevents the width of the current layer from falling below d_e, which is required for onset of the electron shear flow instability. The electron heating at the x line also suppresses the onset of the Buneman instability. Electron drift speeds in the center of the current sheet are comparable with but do not exceed the electron thermal velocity of electrons near the x line. No evidence of the Buneman instability and associated anomalous resistivity has been measured.

[5] The present results are limited to the case of no initial out-of-plane (guide) magnetic field. In a subsequent paper we will show that the behavior of the system with a finite guide field is much more dynamic [Drake et al., 2002]. We also note that the conclusion that secondary instabilities do not play an important role during reconnection at late times does not extend to reconnection onset. During substorm onset in the magnetotail, for example, a substantial component of the magnetic field normal to the current sheet is present in the equilibrium [*Pritchett and Coroniti*, 1995]. We have not explored the stability of this equilibrium nor its nonlinear development and therefore cannot comment on the role of secondary instabilities in this configuration.

2. Numerical Techniques

[6] The simulations are performed with a new three-dimensional particle-in-cell code, which evolves the complete Maxwell equations and the relativistic particle motion in time. Faraday's law and Ampère's law are treated with a trapezoidal leapfrog scheme, and the particles are stepped according to the well-known Boris algorithm [*Birdsall and Langdon*, 1991]. Although the time evolution of the electric field is fully determined by Faraday's law and the continuity equation, discretization errors may accumulate and lead to a secular violation of Gauss's law [*Birdsall and Langdon*, 1991]. As a remedy, Gauss's law must be solved explicitly, leading to a correction for the electric field. The resulting Poisson equation is treated in real space with a three-dimensional multigrid algorithm [*Trottenberg et al.*, 2001]. The computational domain is distributed on the massively parallel computer following a three-dimensional domain decomposition that assigns all particles and fields of a specific subvolume to one processor. The space-scales and timescales in the code are normalized to the ion inertial length, $d_i = c/\omega_{pi}$, and the ion gyrotime, ω_{ci}^{-1}. The code is explicit with separate time steps available for the fields (**E** and **B**) and the particles. The field time step is limited by the Courant condition for light waves, while the particle time step is limited by either the electron plasma frequency ω_{pe} or the electron cyclotron frequency ω_{ce}. The present simulations were carried out on the Cray T3E at the computer center in Garching, which allows for simulations of up to one billion particles on 512 processors.

3. Simulations

[7] We start our discussion with a simulation at parameters similar to those used by *Rogers et al.* [2000]. The initial equilibrium is a double Harris sheet with $B_x/B_0 = \tanh[(y/w_0)] - \tanh[(y - L_y/2)/w_0] - 1$ and $w_0 = d_i$, which is evolved in a box with dimension $L_x = 10\, d_i$, $L_y = 5\, d_i$, $L_z = 1.25\, d_i$ with periodic boundary conditions. The double current sheet provides a system in which the boundary conditions are simple, and the rate of reconnection continues robustly for an extended period of time. This should be contrasted with a single layer with fixed boundary conditions such as was studied in the GEM Reconnection Challenge, where the magnetic island saturates and therefore reconnection halts. Since our goal is to explore the growth of turbulence in the self-generated boundary layers

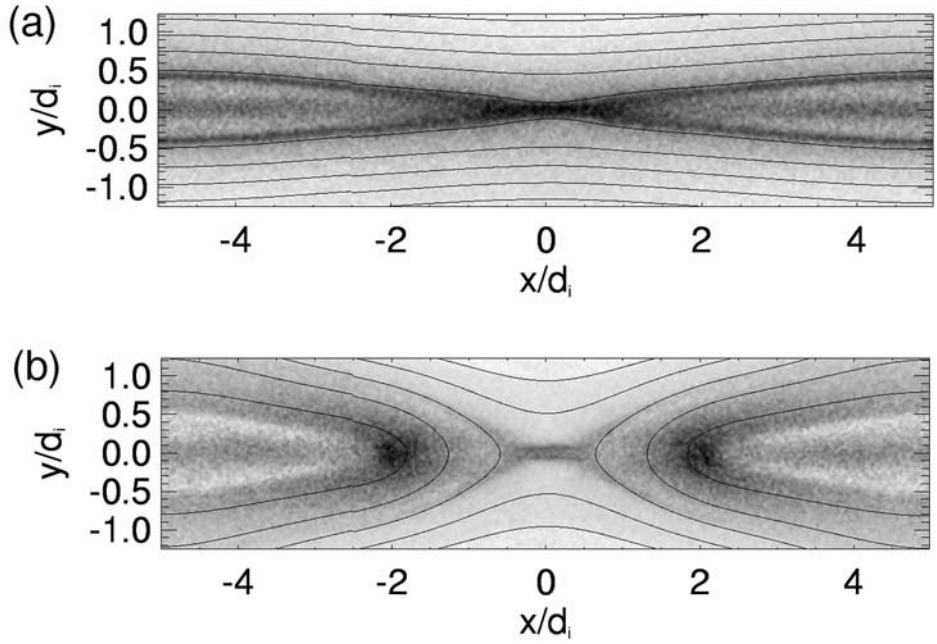

Figure 1. Current density in a 2-D simulation at (a) $t = 7.7/\omega_{ci}$ (b) and $t = 12.9/\omega_{ci}$. Overlaid contour lines correspond to the magnetic flux function ψ.

produced during reconnection, it is essential that reconnection continues as long as possible so that these boundary layers have time to develop. The double current layer is the optimum configuration for this purpose. A uniform density floor of 20% is added to the usual Harris equilibrium density profile so that the maximum density ranges from $1.2\,n_0$ at the center of the current sheet to a minimum of $0.2\,n_0$ outside. The ion inertial length d_i is evaluated at the reference density n_0. The plasma pressure directly results from the force balance relation, which determines the (homogeneous) electron and ion temperature, if the temperature ratio T_i/T_e is given. In our case, unless otherwise specified, we choose $T_i/T_e = 10$, which yields $T_i/m_i v_A^2 = 1/2.2$. The rather small initial electron temperature was chosen to minimize the transverse-scale length of the electron current layer, which is controlled by the electron gyroexcursion near the x line [*Horiuchi and Sato*, 1997] to increase the probability that the layer will be destabilized. We will show, however, that the layer remains stable even as the initial electron temperature tends to zero. Systems with larger values of the electron temperature, which produce broader current layers, are even more stable. The mass ratio is $m_i/m_e = 277.8$, so that the ratio of the electron to ion inertial lengths, d_e/d_i, is 0.06. The speed of light is given by $c/v_A = 15$. For this value of c and the specified mass ratio, $\omega_{ce} = 277.8\,\omega_{ci}$ and $\omega_{pe} = 0.9\,\omega_{ce}$. The ratio of the velocity of light to the electron thermal velocity, c/v_{te}, is 4.22. The computational grid consists of $512 \times 256 \times 64$ collocation points, so the electron Debye length $\lambda_{De} = v_{th,e}/\omega_{pe} = 0.014\,d_i$ is comparable to the grid scale length, a requirement to avoid spurious electron heating. The simulation consists of $\sim$250 million electrons and an equal number of ions, which corresponds to 60 particles per cell in the current layers and 10 particles per cell in the background. The particle time step for the reference simulation is $10^{-3}/\omega_{ci}$, so that both the plasma frequency and the electron cyclotron frequency are resolved by the simulation. The equations for the electromagnetic fields **E**, **B** are substepped, so that the Courant condition on the light velocity does not require additional time for pushing forward the particles. For the parameters of the runs presented in this paper, the field time step is a factor of 10 smaller than that of the particles. To start the reconnection process, the Harris equilibrium is perturbed with magnetic seed islands as initial conditions. No flow conditions are imposed at the boundaries as in some forced reconnection simulations [*Horiuchi and Sato*, 1999]. The initial island width is $\sim 0.4\,d_i$. Perturbations in the plasma density and plasma current are not included. The plasma current is quickly self-generated by the dynamics. The rather large seed islands enable the system to quickly get into the nonlinear reconnection phase, which is of most interest in this study. Such a large seed precludes an exploration of the linear growth of the tearing mode and the competition between the tearing mode and other instabilities in controlling the onset of reconnection which, as discussed previously, is not the primary topic of this work.

[8] For reference, we perform a two-dimensional simulation with the same parameters and box dimensions in the x and y directions and with $\sim$6 million particles. In the 2-D case the initial magnetic perturbation leads to the formation of an X point at an early time (Figure 1a) with current sheets that remain quiescent even during the phase of fast reconnection (Figure 1b). The time evolution of the magnetic flux ψ is shown in Figure 2. Note that the slope of the curve, which is the reconnection electric field, has a maximum of 0.2, which is comparable to that found earlier in the GEM Reconnection Challenge.

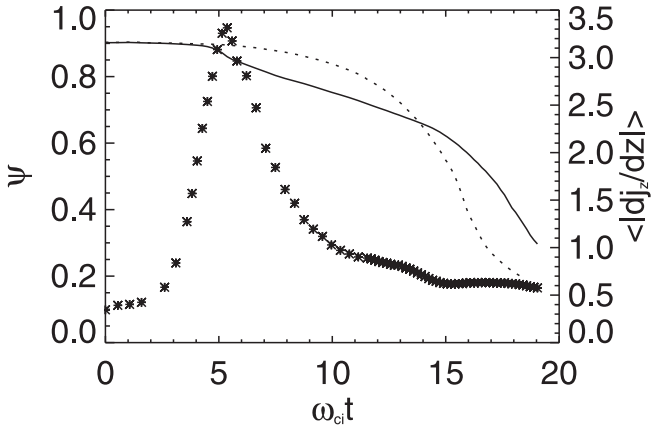

Figure 2. Time evolution of the magnetic flux in the 3-D (solid line) and in the 2-D (dashed line) case and of the current fluctuations along z (stars). The flux is calculated according to $\Psi = [\psi(0, 0) - \psi(0, L_y/2)]/4 + [\psi(L_x/2, 0) - \psi(L_x/2, L_y/2)]/4$; thus the total magnetic flux is reconnected when $\Psi = 0$. The current fluctuations are calculated by averaging $|dJ_z/dz|$ over the whole simulation domain.

[9] In the 3-D case, by contrast, the Harris sheet becomes unstable at a very early time, leading to a strongly distorted current distribution even before the fast reconnection starts (Figure 3a). To compare with the 2-D simulation and to compute an effective reconnection electric field, we define a 2-D flux function ψ with the equation $\nabla^2\psi = \langle J_z\rangle_z$, where $\langle\rangle_z$ denotes an average over the z direction. The z-averaged magnetic field $\langle \mathbf{B}\rangle_z$ then satisfies the equation $\langle \mathbf{B}\rangle_z = \hat{z} \times \nabla\psi$. The X-point structure of the resulting 2-D flux function is shown in Figure 3a. The structure of this mean magnetic field is not strongly altered by the development of the z-dependent fluctuations. Figure 4a shows the density at the same time in the $y - z$ plane cutting through the X point. The instability is located where the density gradients are largest, so that the main current filament in the center of the sheet remains nearly unperturbed and retains its initial 2-D structure. The current fluctuations along the z direction coincide with a transient acceleration of the reconnection rate compared with the 2-D case (Figure 2). As reconnection proceeds, however, the quasi 2-D structure of the current distribution is re-established (Figure 3b) as the z-dependent fluctuations decay to a comparatively low level (Figure 2). Near the x line the electron current flows in a straight narrow channel (Figure 4c), which is embedded in a much wider density layer (Figure 4b). In contrast, the fluctuations continue to be driven along the boundary between the inflow and outflow regions, just downstream of the separatrix (Figure 4d). Overall, the 3-D effects remain surprisingly weak, and the evolution closely resembles that of the 2-D system. Buneman, electron shear flow, and drift kink instabilities are completely absent from our kinetic simulations (note the quiescent current channel in Figure 4c). The behavior of the lower hybrid instability, which is responsible for the boundary layer fluctuations, is consistent with fluid predictions as will be discussed now in more detail but does not significantly impact the rate of reconnection.

4. Lower Hybrid Drift Instability

[10] The instability that is observed around $t = 5/\omega_{ci}$ in the 3-D run exhibits the main properties of the lower hybrid drift (LHD) instability. The LHD mode is expected to be

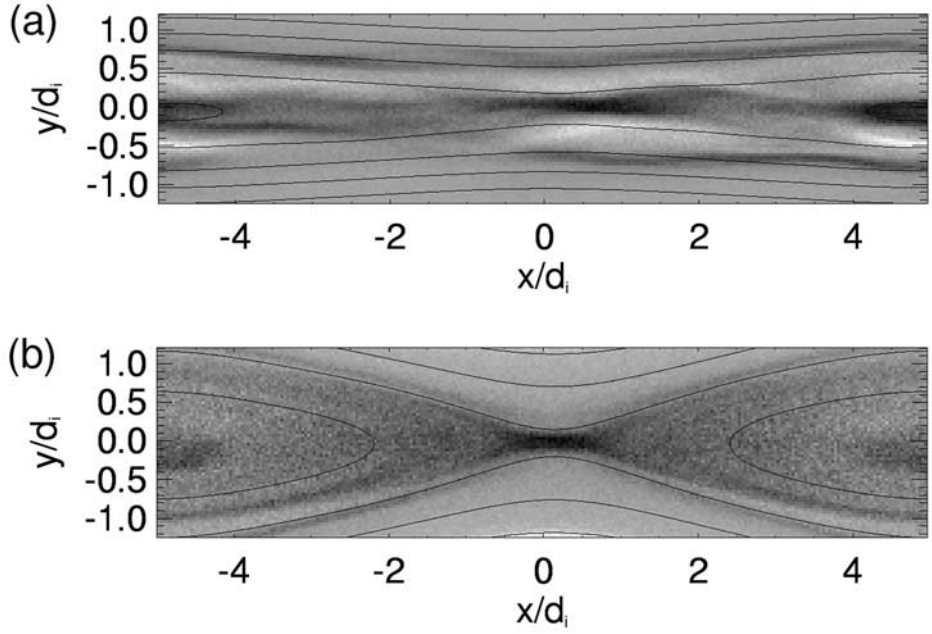

Figure 3. From the 3-D simulation. Current density in the $x - y$ plane at $z = 0$ at (a) $t = 5.4/\omega_{ci}$ and (b) $t = 12.9/\omega_{ci}$. The magnetic flux function ψ (contour lines) is calculated by averaging over z.

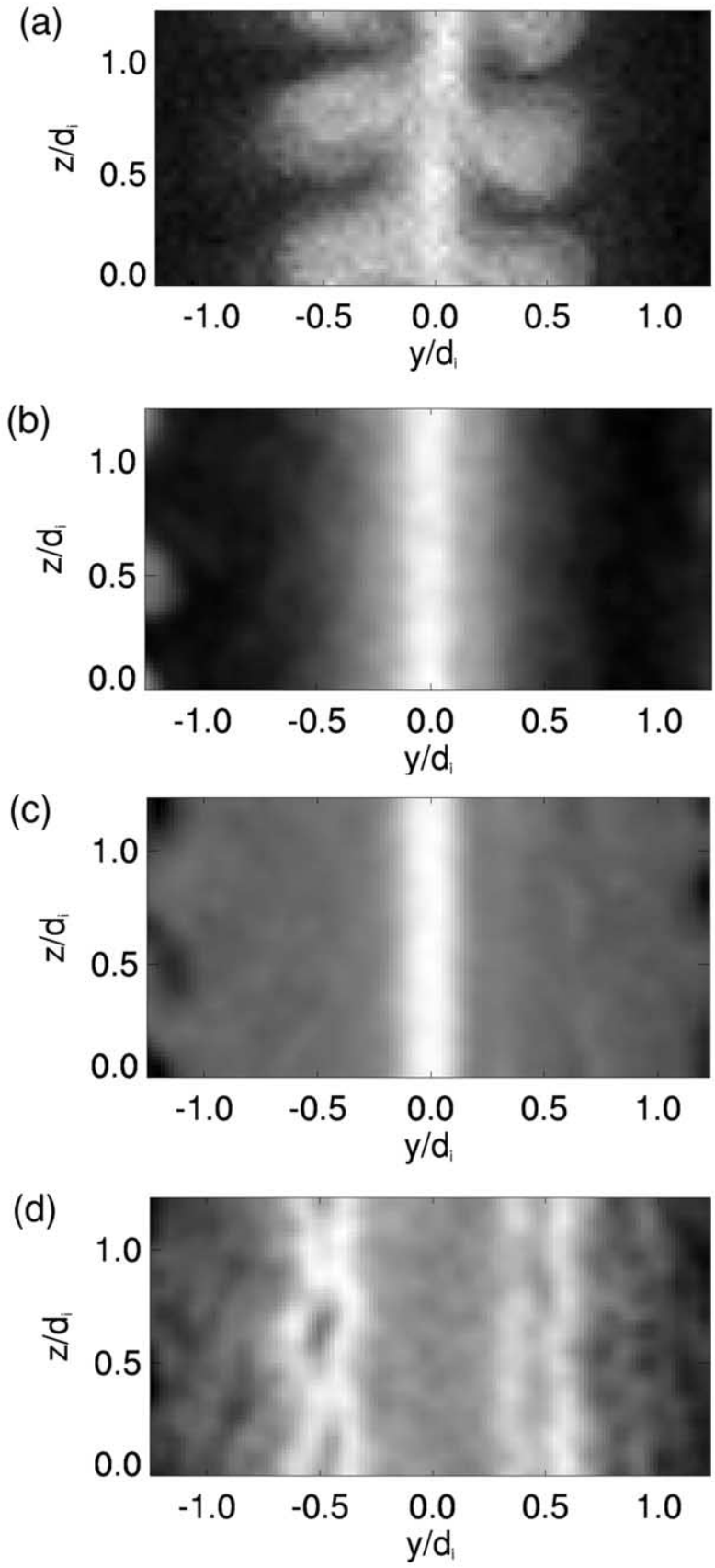

Figure 4. From the 3-D simulation. Electron density in the $y - z$ plane at the x line at (a) $t = 5.4/\omega_{ci}$ and (b) $t = 12.9/\omega_{ci}$. The electron velocity v_{ez} in the $y - z$ plane at $t = 12.9/\omega_{ci}$ at (c) the x line and at (d) $x = 1.5\ d_i$.

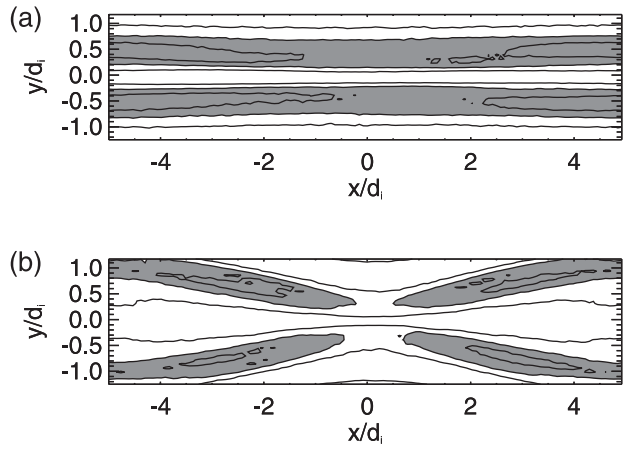

Figure 5. Lower hybrid drift (LHD) unstable regions at (a) $t = 3.8/\omega_{ci}$ and (b) $t = 15.2/\omega_{ci}$. Plotted are contour lines of the two-fluid stability parameter $\rho_{si}/(1 + \beta/2)/L_n$ at the levels 0.5, 1, and 1.5. In the shaded regions the stability parameter is larger than 1, indicating that the LHD mode is expected to be unstable.

destabilized at the location of the steepest pressure gradient [*Huba et al.*, 1980; *Brackbill et al.*, 1984; *Horiuchi and Sato*, 1999] and well separated from the high-β region around the center of the current sheet, consistent with Figure 3a. Here $\beta = 8\pi n(T_e + T_i)/B^2$. At gradients $L_n \ll c/\omega_{pi}$, a two-fluid analysis [*Rogers et al.*, 2000] predicts unstable eigenmodes in the range $(1 + \beta/2)L_n/\rho_{si} \lesssim k\rho_{se} \lesssim 1$ with $\rho_{s\alpha}^2 = d_\alpha^2\beta/2$. Figure 5a shows that during the early phase of the simulation the LHD mode is expected to be unstable along the entire Harris sheet, including the x line, consistent with Figure 4a. As reconnection proceeds, the LHD mode is suppressed in the vicinity of the X point (Figure 5b), and the current sheet becomes quiescent in this location (Figures 4b and 4c). Figure 6b is a cut of the density through the x line at late time. Reconnection actually steepens the density profile just outside the electron current layer, but the plasma β in this region is high, and as a consequence, the LHD mode remains stable. Further upstream from the x line where β is smaller, the gradients in density decrease as reconnection proceeds, so that LHD remains stable in the entire region around the x line. Downstream along the separatrices, however, where β is modest, the condition for instability is still satisfied, consistent with the observed mode activity at this location (Figure 4d). Finally, the wavelength of the LHD mode is given approximately by $k\rho_{se} \simeq 1$, which yields $\lambda/d_i \simeq 0.3$, in excellent agreement with Figure 4a.

[11] In our 3-D reference simulation the initial profiles considerably exceed the stability limit for the LHD instability, as shown in Figure 5a. To address the question whether an initially weaker density gradient would self-steepen as reconnection proceeds, thereby triggering the LHD mode even if the initial equilibrium were stable, we completed a 2-D simulation with a larger background density. In this run, all parameters are as in our previous 2-D reference simulation except for the ratio $n_{\max}/n_{\min}$, which previously was 6 and is now reduced to 2 by a larger background density. The increased background density lowers the density gradient and thus stabilizes the LHD instability. As the simulation proceeds, the gradients near the x line evolve as in the reference simulation and drive the parameters even further into the regime where the LHD mode is stable. Along the separatrix toward the O line, however, the gradients moderately steepen, and eventually the stability threshold is exceeded. Thus self-consistent steepening of the profiles and subsequent destabilization of the LHD mode appears likely along the separatrix downstream from the x line but is unlikely in the vicinity of the X point, consistent with the earlier two-fluid simulations [*Rogers et al.*, 2000].

5. Stability of Electron Current Sheets

[12] An important difference between the present kinetic simulations and earlier kinetic and two-fluid results [*Rogers et al.*, 2000] is the fact that the electron current sheet remains completely stable. There is no evidence for the drift kink, electron shear flow instabilities, or Buneman instabilities. The absence of the drift-kink instability is consistent with calculations of *Daughton* [1999], who showed that the instability was very weak for the large

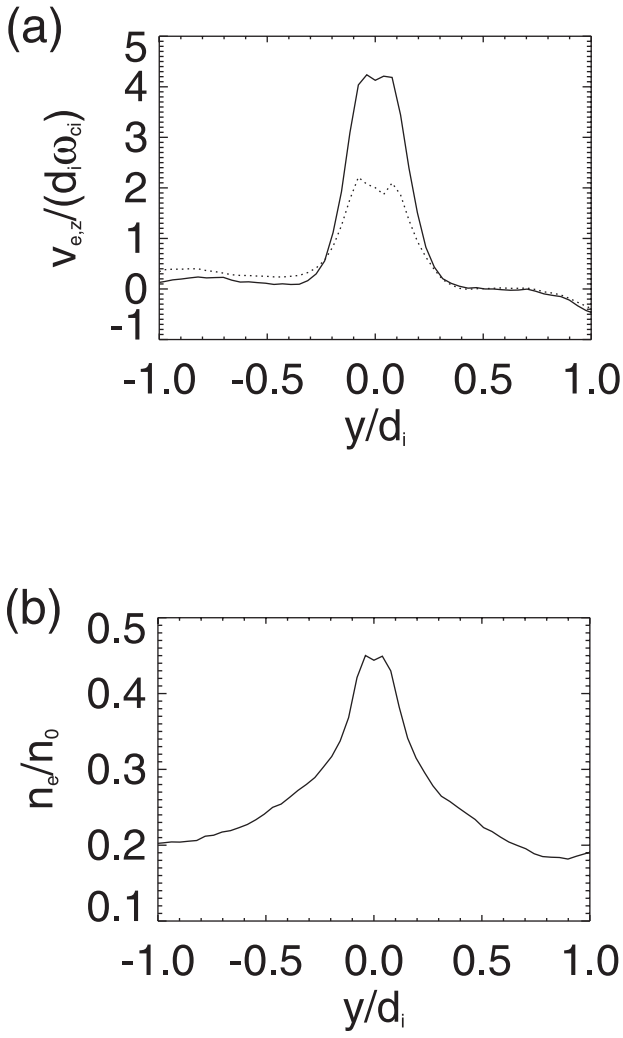

Figure 6. Electron current layer in the vicinity of the x line at $t = 14.75/\omega_{ci}$. (a) Mean velocity $v_{e,z}$ (solid line) and $\vec{E} \times \vec{B}$ velocity (dashed line). (b) Electron density profile.

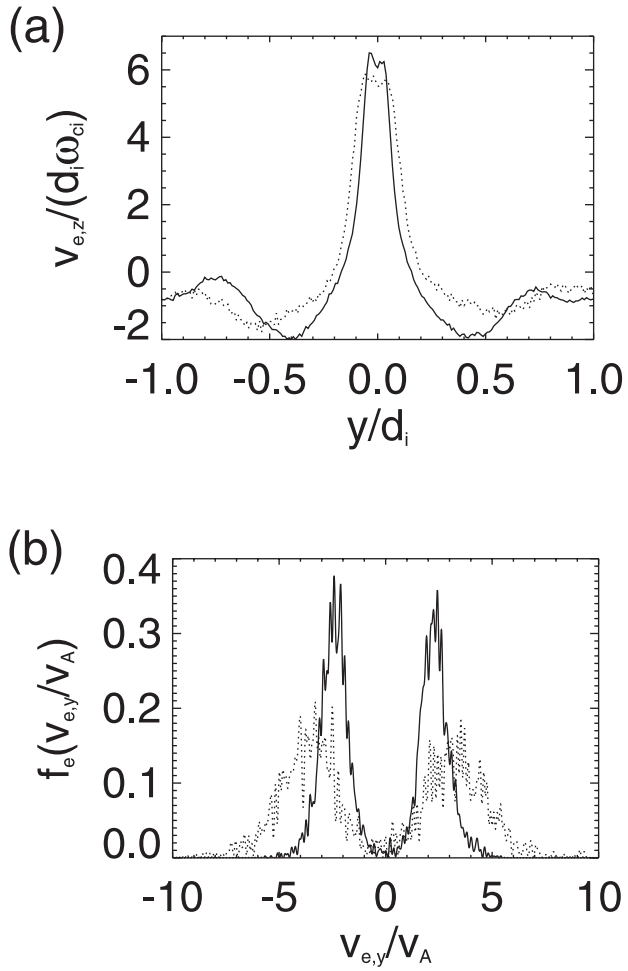

Figure 7. (a) Electron flow velocity $v_{e,z}$ versus y across the x line. (b) Electron distribution function $f_e(v_y)$ at the x line for two initial electron temperatures, 0.01 (solid line) and 0.04 (dashed line).

ion-electron mass ratios, which characterize space and solar plasmas. At a mass ratio significantly below that of the reference run (m_i/m_e = 25), kinking of the current channel was observed, consistent with the Daughton theory. We note, however, that the length of the simulation domain in the z direction was only 1.25 d_i. We cannot be sure that instabilities at a longer wavelength than the box size in this direction are not unstable. However, at late time the current sheet collapses to a width of several d_e. This can be seen in Figure 4c, where the electron mean velocity rises from zero to 3.5 v_A over a distance of $\sim$3 d_e. Figure 6 shows the density and velocity profiles for a similar situation. In Daughton's theory of the kinetic kink instability the growth rate maximizes for $k_z w \sim 1$, with w the width of the current layer, and falls off at longer wavelength. Because of the strong compression of the current layer at late time, the most unstable modes, corresponding to $k_z \sim 0.3/d_e$, fall within the range of wavelengths modeled by the grid. It therefore seems doubtful that an increased computational length in the z direction would allow the drift kink instability to grow.

[13] The absence of electron shear flow instabilities is perhaps surprising in light of the narrow current layers which develop near the x line. A simple Harris current sheet of such thickness would be strongly unstable. However, the current sheet differs significantly from the initial Harris equilibrium. Although in the Harris sheet the current results from the diamagnetic drift of electrons and ions (at our temperature ratio almost the entire initial current is carried by the ions), we now find a significant electric field along the y direction. The associated $\vec{E} \times \vec{B}$ drift carries a large fraction of the overall electron current, as shown in Figure 6a. The dynamics of such a thin electron current sheet with a modest density variation is approximately described by electron magnetohydrodynamics [*Biskamp et al.*, 1995]. In the 2-D limit the current sheet satisfies the equation $d/dt(1 - d_e^2\nabla^2)\phi = 0$, with $d/dt = \partial/\partial t + \vec{v} \cdot \nabla$, $\vec{v} = \vec{z} \times \nabla\phi$. At scales $kd_e \gg 1$, this equation becomes the Euler equation $d\vec{v}_e/dt = 0$, implying that a sheared velocity field becomes Kelvin-Helmholtz unstable. If the width of the current layer approaches the electron inertial length, the Kelvin-Helmholtz instability is suppressed. Simulations of the electron magnetohydrodynamics (EMHD) system exhibit complete stabilization if the width of the current sheet exceeds 0.7 d_e. To verify this result for the kinetic case, we study the two-dimensional evolution of an electron current sheet of width d_e and a peak velocity $v_{\max} = d_e\omega_{ce}$ with a neutralizing background of immobile ions (d_e and ω_{ce} are measured far away from the current sheet). The current sheet kinks at a wavelength of $\sim$7 d_e and a growth rate $\gamma \simeq \omega_{ce}/30$. This growth rate is much smaller than what is expected for the standard Kelvin-Helmholtz instability, consistent with stabilization at the d_e scale. Changing the width of the current layer has a strong impact on the growth rate; increasing the width by 17% decreases the growth rate by a factor of $\sim$2, whereas decreasing the width by the same amount doubles the growth rate. Thus the stability of the electron current layer to electron velocity shear instabilities is a consequence of the width of the layer being larger than d_e.

[14] In a kinetic model this width is linked to the gyro excursion of electrons bouncing across the low magnetic field region near the x line, which depends on the electron temperature in this region [*Horiuchi and Sato*, 1997]. The width of the current layer in Figure 6a is consistent with the electron temperature at the start of the simulation. One

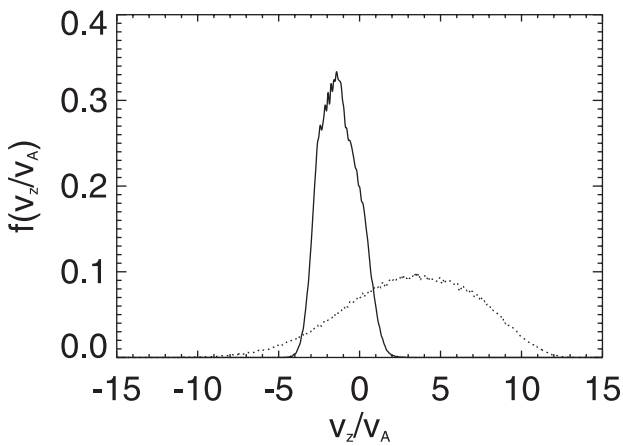

Figure 8. Ion (solid line) and electron (dashed line) velocity distribution along the z direction and within the current layer at $t = 0.5/\omega_{ci}$.

might therefore expect that a reduction of the electron temperature below $T_e/T_i = 0.1$ would result in a reduced current layer width and therefore instability. Carrying out a 3-D simulation with even smaller electron temperature to test this idea is not possible because of the requirement that the Debye length be resolved to avoid numerical electron heating. The associated decrease in the grid size makes this computation prohibitive within the limitations of the present computational resources.

[15] There are, however, theoretical ideas for believing that the electron current layer thickness in kinetic models cannot fall below d_e even when the upstream electron temperature is zero. The outflow velocity from the x line has been shown to scale like the electron Alfven speed V_{Ae} [*Shay et al.*, 2001]. The inflow velocity, just upstream of the electron current layer, scales similarly when the electron upstream temperature is small. As the electrons enter the low magnetic field region of the current layer, they become demagnetized and move to the opposite side of the current layer until the magnetic field is strong enough to reflect them [*Burkhart et al.*, 1990]. The electrons flowing toward the x line from the opposite side of the current layer do likewise with the result that the electrons counterstream across the current layer, creating an effective electron thermal velocity which scales like the V_{Ae}. The electron excursion during the bounce across the current layer is of order $V_{Ae}\omega_{ce} = d_e$, indicating that the electron current layer cannot fall below d_e even when the electron thermal velocity approaches zero. To test this idea, we have carried out a series of 2-D simulations with varying values of initial electron temperature. In Figure 7 we plot the mean electron drift velocity, $v_{e,z}$, versus y across the x line and the electron distribution function, $f_e(v_y)$, at the x line for two values of the electron temperature (normalized to $m_i v_A^2$), 0.04, and 0.01. For the larger initial temperature the counterstreaming at the x line is modest, and the width of the current layer is largely determined by the initial temperature. For the lower initial temperature the velocity space separation of the counterstreaming beams is substantial. The excursion of an electron with a streaming velocity $v_y = 4.0v_A$, corresponding to Figure 7b, and the measured magnetic field gradient dB_x/dy is $0.1\,d_i$, which is the width of the current layer in Figure 7a. Thus the width of the layer is determined by the streaming velocity rather than by the inflow temperature. The width of the electron current layer therefore does not fall below d_e in a kinetic model, so that electron Kelvin-Helmholtz-type instabilities in reversed magnetic field configurations are completely stable, consistent with the present simulations.

[16] In addition to current gradient-driven modes, a Buneman instability might arise in the current layer due to the large relative velocity of electrons and ions. For cold electron and ion beams the Buneman instability obeys the dispersion relation $1 = \omega_{pi}^2/(\omega - kv_i)^2 + \omega_{pe}^2/(\omega - kv_e)^2$. It is well known, however, that this relation becomes invalid if the electron thermal velocity is not negligible compared with the beam velocity. Figure 8 shows the ion and electron velocity distribution within the current layer, demonstrating that the streaming velocity of the electrons is comparable to the thermal velocity of the electrons. Nevertheless, the thermal spread of the electrons is sufficient to stabilize the Buneman instability [*Krall and Trivelpiece*, 1973]. For the parameters of our simulation but smaller electron temperature $T_e \simeq T_i/100$, a one-dimensional electrostatic simulation performed with our code reproduces the predicted, most unstable wavelength of the Buneman instability. At the electron temperature of our 3-D simulation, by contrast, the 1-D electrostatic simulation does not exhibit any indication of a two-stream instability. In our complete electromagnetic 3-D run we observe a small perturbation in the current sheets which might be a remnant of a Buneman instability. Consistent with our 1-D electrostatic tests, the perturbations remain weak.

6. Conclusions

[17] Full particle simulations in three dimensions show that boundary layers flanking the outflow region during collisionless reconnection form and sustain large density gradients and destabilize lower hybrid drift modes, in agreement with previous two-fluid results. In the vicinity of the x line, however, the density gradients steepen only in the region of high β, where the LHD instability cannot exist. Thus the LHD fluctuations are suppressed in the vicinity of the x line. Though reconnection leads to the formation of a thin electron current sheet at the x line, we do not observe sheets with a width below the electron inertial length d_e. As a consequence, electron shear flow driven instabilities are absent. Test runs show that further narrowing the electron current sheet destabilizes a Kelvin-Helmholtz-like kink mode as expected from electron magnetohydrodynamics. We argue, however, that such narrow current sheets will never form during reconnection because the intrinsic heating of electrons as they flow into the low magnetic field near the x line causes the electron gyro-excursion across the x line to exceed d_e. Therefore the width of self-consistently formed current sheets remains in excess of d_e, implying that electron shear flow driven modes are unimportant. Similar electron self-heating appears to suppress the Buneman instability. Finally, at the large ion to electron mass ratios (277.8) utilized in the present simulations, the drift kink instability is suppressed, consistent with the linear theory of Daughton. As a consequence, our 3-D particle simulations of collisionless reconnection are in remarkably good agreement with the 2-D limit, much better than expected from two-fluid simulations and earlier full particle simulations with reduced ion to electron mass. The weak lower hybrid drift instabilities, which survive along the boundaries of the outflow region, play a very limited role in the reconnection process.

[18] **Acknowledgments.** This work was supported by NSF grant ATM0078435 and NASA grants NAG58459 and NAG59108.

[19] Janet G. Luhmann thanks Ken Nishikawa and another referee for their assistance in evaluating this paper.

References

Birdsall, C. K., and A. B. Langdon, *Plasma Physics via Computer Simulation*, McGraw-Hill, New York, 1991.

Birn, J., et al., Geospace Environmental Modeling (GEM) Magnetic Reconnection Challenge, *J. Geophys. Res.*, *106*, 3715, 2001.

Biskamp, D., E. Schwarz, and J. F. Drake, Ion-controlled collisionless magnetic reconnection, *Phys. Rev. Lett.*, *75*, 3850, 1995.

Brackbill, J. U., D. W. Forslund, K. B. Quest, and D. Winske, Nonlinear evolution of the lower-hybrid drift instability, *Phys. Fluids*, *27*, 2682, 1984.

Büchner, J., Three-dimensional magnetic reconnection in astrophysical plasmas—Kinetic approach, *Astrophys. Space Sci.*, *264*, 2542, 1999.

Burkhart, G. R., J. F. Drake, and J. Chen, Magnetic reconnection in collisionless plasmas: Prescribed fields, *J. Geophys. Res.*, *95*, 18,833, 1990.

Daughton, W., The unstable eigenmodes of a neutral sheet, *Phys. Plasmas*, *6*, 1329, 1999.

Drake, J. F., D. Biskamp, and A. Zeiler, Breakup of the electron current layer during 3-D collisionless magnetic reconnection, *Geophys. Res. Lett.*, *24*, 2921, 1997.

Drake J. F., et al., Formation of electron-holes and particle energization during magnetic reconnection, submitted to *Science*, 2002.

Hesse, M., M. M. Kuznetsova, and J. Birn, Collisionless magnetic reconnection in three dimensions: The growth of oblique modes in PIC simulations, *Eos Trans. AGU*, Spring Meet. Suppl., Abstract SM31A-04, 2001.

Horiuchi, R., and T. Sato, Particle simulation study of collisionless driven reconnection in a sheared magnetic field, *Phys. Plasmas*, *4*, 277, 1997.

Horiuchi, R., and T. Sato, Three-dimensional particle simulation of plasma instabilities and collisionless reconnection in a current sheet, *Phys. Plasmas*, *6*, 4565, 1999.

Huba, J. D., J. F. Drake, and N. T. Gladd, Lower-hybrid-drift instability in field reversed plasmas, *Phys. Fluids*, *23*, 552, 1980.

Krall, N. A., and A. W. Trivelpiece, *Principles of Plasma Physics*, McGraw-Hill, New York, 1973.

Ozaki, M., T. Sato, R. Horiuchi, and C. S. Group, Electromagnetic instability and anomalous resistivity in a magnetic neutral sheet, *Phys. Plasmas*, *3*, 2265, 1996.

Pritchett, P. L., Collisionless magnetic reconnection in a 3-D open system, *Eos Trans. AGU*, Spring Meet. Suppl., Abstract SM22A-09, 2001.

Pritchett, P. L., and F. V. Coroniti, Formation of thin current sheets during plasma sheet convection, *J. Geophys. Res.*, *100*, 23,551, 1995.

Pritchett, P. L., and F. V. Coroniti, The role of drift kink mode in destabilizing thin current sheets, *J. Geomagn. Geoelectr.*, *48*, 833, 1996.

Pritchett, P. L., and F. V. Coroniti, Kinetic simulations of 3-D reconnection and magnetotail disruptions, *Earth Planets Space*, *53*, 635, 2001.

Rogers, B. N., J. F. Drake, and M. A. Shay, The onset of turbulence in collisionless magnetic reconnection, *Geophys. Res. Lett.*, *27*, 3157, 2000.

Shay, M. A., J. F. Drake, B. N. Rogers, and R. E. Denton, Alfvenic collisionless magnetic reconnection and the Hall term, *J. Geophys. Res.*, *106*, 3759, 2001.

Trottenberg, U., C. W. Oosterlee, and A. Schüller, *Multigrid*, Academic, San Diego, Calif., 2001.

Zhu, Z., and R. M. Winglee, Tearing instability, flux ropes, and kinetic current sheet kink instability in the Earth's magnetotail: A three-dimensional perspective from particle simulations, *J. Geophys. Res.*, *101*, 4885, 1996.

D. Biskamp and A. Zeiler, Max-Planck-Institut für Plasmaphysik, Centre for Interdisciplinary Plasma Science, Karl-Schwarzschild Str. 1, Garching D-85748, Germany. (dfb@ipp.mpg.de; zeiler@vohloh.de)

J. F. Drake, B. N. Rogers, and M. A. Shay, Institute for Plasma Research, University of Maryland, College Park, MD 20742, USA. (drake@glue.umd.edu; rogers@plasma.umd.edu; shay@glue.umd.edu)

M. Scholer, Max-Planck-Institut für Extraterrestrische Physik, Centre for Interdisciplinary Plasma Science, Karl Schwarzschild Str. 1, P.O. Box 1603, Garching-bei-München D-85740, Germany. (mbs@mpe.mpg.de)